Journal of the American Heart Association

ORIGINAL RESEARCH

Comparative Analysis of Atrial Electrophysiology Across Animal Species and Humans: Enhancing Translation in Atrial Arrhythmia Research

Amelie Paasche; Felix Wiedmann, MD; Christian Goetz, MSc; Leo Weirauch; Lize-Maria Verhaeghe, MSc; Annelies Decloedt, PhD; Manuel Kraft, PhD; Max Jamros; Anna L. Meyer, MD; Norbert Frey, MD; Marcin Zaradzki, MD; Matthias Karck, MD; Gunther van Loon, PhD; Axel Loewe, PhD; Constanze Schmidt, MD

BACKGROUND: Atrial arrhythmias relevantly contribute to global morbidity and death and have been extensively studied in experimental models. However, electrophysiological disparities between animal models and humans often hinder the translation of experimental findings. This study aims to systematically characterize species-specific atrial electrophysiology to improve translation.

METHODS: Atrial tissue samples were obtained from patients undergoing open heart surgery and from mice, rats, pigs, and horses, and were characterized at the cellular electrophysiological and transcriptomic level using uniform protocols. To assess the correlation of functional and transcriptomic features, action potentials were simulated from ion channel expression profiles using in silico models.

RESULTS: Porcine atrial cardiomyocytes closely resembled human cells in depolarization characteristics, whereas rodents exhibited marked differences. Human atrial action potentials showed pronounced early repolarization, which was not reproduced in other species and corresponded to a greater contribution of the I_{Kur} gene group. Late repolarization, reflected by action potential duration at 90% repolarization, scaled with species and cardiomyocyte size, with humans ranging between rodents and pigs. Sex-specific differences in repolarization observed in humans were represented in pigs but not in rodents. Chamber-specific differences between left and right atrial cardiomyocytes were reflected in in silico simulations on the basis of ion channel expression.

CONCLUSIONS: This study provides a reference for species-specific atrial action potential characteristics, linking functional properties to transcriptomic ion channel expression. It further demonstrates that relative changes in action potential parameters can be inferred from transcriptomic data using in silico simulations. These findings support more accurate interpretation and translation of animal experimental data to human atrial electrophysiology.

Key Words: action potential ■ atrial electrophysiology ■ ion channels ■ patch clamp

Atrial arrhythmias pose a significant health challenge in an aging society, occurring both independently and in conjunction with various cardiovascular diseases. Atrial fibrillation (AF) stands as the most prevalent sustained cardiac arrhythmia, with an estimated lifetime risk of 1 in 3 to 4 individuals,

Correspondence to: Constanze Schmidt, MD, FESC, FEHRA, Department of Cardiology and Pneumology, University Medical Center Goettingen, Robert-Koch-Street 40, D-37075 Goettingen, Germany. Email: constanze.schmidt@med.uni-goettingen.de

Supplemental Material is available at https://www.ahajournals.org/doi/suppl/10.1161/JAHA.125.048989

This manuscript was sent to Sakima A. Smith, MD, MPH, Associate Editor, for review by expert referees, editorial decision, and final disposition.

For Sources of Funding and Disclosures, see page 15.

JAHA is available at: www.ahajournals.org/journal/jaha

CLINICAL PERSPECTIVE

What Is New?

- We present the first data set comprising atrial action potential recordings from human patients, mice, rats, pigs, and horses, obtained using standardized experimental protocols across species.
- We introduce a novel approach to compare atrial ion channel expression profiles across species, thereby linking functional electrophysiological and transcriptomic data.

What Are the Clinical Implications?

- This study provides new insights into species-specific atrial electrophysiology at both the functional and transcriptomic levels to facilitate the translation of experimental findings from animal models into clinical practice in atrial arrhythmia research.

Nonstandard Abbreviations and Acronyms

AP	action potential
APA	action potential amplitude
APD	action potential duration
APD_{30}	action potential duration at 30% repolarization
APD_{50}	action potential duration at 50% repolarization
APD_{90}	action potential duration at 90% repolarization
BCL	basic cycle length
RMP	resting membrane potential
TPM	transcripts per million

and relevantly contributes to global morbidity and death.[1] Additionally, atrial arrhythmias have often been underestimated as substantial contributors to ventricular conditions.[2,3] Despite decades of intensive research, satisfactory therapeutic options remain elusive. Effective pharmacological treatments are still lacking, and recurrence rates following catheter ablation procedures remain high.[4,5]

Numerous animal models of AF have been established, encompassing a wide range of species, including mice, rats, guinea pigs, rabbits, pigs, goats, sheep, and dogs. Recent comprehensive literature reviews by Odening et al[6] and Schüttler et al[7] highlight the unique advantages and limitations of each model. Various methods, such as tachypacing, cardiac hypertrophy (eg, via transverse aortic constriction), ventricular ischemia, cardiac inflammation, and transgenic models are used to induce arrhythmias. Collectively, animal models have significantly advanced our understanding of pathomechanisms underlying structural and electrical remodeling in AF. A hallmark of AF-associated atrial remodeling is the alteration of electrophysiological properties in individual cardiomyocytes. Modulation of specific ion channels and currents has been shown to result in atrial action potential (AP) shortening and the generation of afterdepolarizations, which can facilitate the establishment of electrical reentries.[8–10]

However, as cellular studies often rely on experiments in nonhuman cardiomyocytes, the translation of preclinical insights into clinical practice presents significant challenges. While the complexity and multifactorial nature of the disease contribute to this translational gap, another critical factor is the electrophysiological differences between animal models and human patients. The choice of species for experimental studies can strongly influence the relevance and applicability of findings to the human clinical setting.

Therefore, it is essential to identify and understand differences and similarities in cardiac electrophysiology across species. Significant interspecies variations in APs and ion currents, which shape the AP, have been documented.[10] Although previous review articles have provided valuable insights into species-specific electrophysiology, many studies have primarily focused on ventricular electrophysiology. Moreover, they often face challenges in integrating data from heterogeneous studies.[6,7] Inconsistencies in, for example, the methodologies for measuring APs can complicate comparisons. Consistent data on characteristic species-dependent differences in atrial APs and the underlying transmembrane currents are lacking.

Despite the widespread use of rodents as animal models in arrhythmia research, their transferability to human physiology is limited due to pronounced anatomic and electrophysiological differences.[6,11,12] While pigs have a heart anatomy closely resembling that of humans and horses can spontaneously develop AF, increasing costs and ethical restrictions for large-animal research contribute to a continued preference for mice and rats in arrhythmia studies.[6,7] Therefore, it is crucial to raise awareness for the limitations of each animal model and identify specifics of the human atrial AP.

In this study, atrial APs from mice, rats, pigs, horses, and humans in sinus rhythm were recorded using standardized experimental protocols. Electrophysiological data at the single-cell level were integrated with transcriptomic data at the atrial tissue level to identify correlations between functional parameters and ion channel expression profiles. Understanding species-specific characteristics at both levels can enhance the translation of experimental findings in atrial arrhythmia research.

METHODS

The data that support the findings of this study are available from the corresponding author upon reasonable request.

Study Patients

A total of 74 patients undergoing open heart surgery for procedures like coronary artery bypass grafting or heart valve repair were enrolled in the study (Table). All patients were in sinus rhythm, a history of AF was ruled out. Sixteen patients (12 men, 4 women) were used for cardiomyocyte isolation and cellular electrophysiological characterization, 15 patients (12 men, 3 women) were used for RNA isolation and sequencing, and 59 patients (45 men, 14 women) were used for the analysis of ECGs. All patients provided written informed consent. The study protocol, which involved the use of human tissue samples, received approval from the Ethics Committee of the Medical Faculty at Heidelberg University in Germany (Approval No. S-017/2013) and was conducted in adherence to the principles outlined in the Declaration of Helsinki. Human right atrial (RA) tissue samples were obtained during standard cannulation, whereas left atrial (LA) samples were collected from the free wall during left atriotomy performed for mitral valve reconstruction. After excision of the atrial tissue sample, it was kept in a 2,3-butanedionmonoxime–containing cardioplegic solution (in mmol/L: 30 2,3-butanedionmonoxime, 20 glucose, 10 KCl, 1.2 KH_2PO_4, 5 $MgSO_4$, 5 MOPS, 100 NaCl, 5 taurine; pH 7.0) at 4 to 8 °C for transport, and subjected to cardiomyocyte isolation within 30 minutes after excision.

Animal Handling

Animal experiments were conducted in compliance with guidelines set forth by the US National Institutes of Health (NIH Publication No. 86-23), the

Table. Baseline Characteristics of Study Patients

	Patch clamp analysis (n=16)	RNA sequencing analysis (n=15)	ECG analysis (n=59)
Demographics			
Age, y, mean±SEM	63.7±2.8	69.9±2.5	65.5±1.3
Female sex, n (%)	4 (25.0)	3 (20.0)	14 (23.7)
Height, cm, mean±SEM	175.3±2.3	173.3±1.5	174.9±1.1
Body weight, kg, mean±SEM	82.1±4.6	83.4±3.9	83.4±2.4
Body mass index, kg/m^2, mean±SEM	26.5±1.1	27.7±1.2	27.1±0.7
Heart rhythm			
Sinus rhythm, n (%)	16 (100)	15 (100)	59 (100)
Echocardiography			
Left ventricular ejection fraction, %, mean±SEM	53.4±3.0	45±4.1	56.3±1.3*
Left atrial diameter, mm, mean±SEM	41.3±1.7	43.7±1.6	39.4±0.7*
Medical history, n (%)			
Hypertension	16 (100)	15 (100)	49 (83.1)
Type 2 diabetes	4 (25.0)	4 (26.7)	13 (22.0)
Coronary heart disease	14 (87.5)	14 (93.3)	48 (81.4)
Hyperlipidemia	15 (93.8)	11 (73.3)	46 (78.0)
Concomitant medication, n (%)			
Angiotensin-converting enzyme inhibitors	10 (62.5)	4 (26.7)	23 (39.0)
Angiotensin II receptor type 1 antagonists	3 (18.8)	3 (20.0)	22 (37.3)
Valsartan+sacubitril	3 (18.8)	0 (0)	3 (5.1)
Statins	15 (93.8)	11 (73.3)	46 (78.0)
Digitalis glycosides	0 (0)	0 (0)	0 (0)
β Blockers	12 (75.0)	9 (60.0)	34 (57.6)
Sodium–glucose linked transporter 2 inhibitors	2 (12.5)	0 (0)	5 (8.5)
Class I/III antiarrhythmic drugs	0 (0)	0 (0)	0 (0)

*$P<0.05$ vs patients for RNA sequencing analysis from ordinary 1-way ANOVA followed by Tukey multiple comparisons procedure for continuous variables and from Fisher's exact test for categorical variables.

EU Directive 2010/63/EU, and German laws for animal protection. Approval was obtained from local Animal Welfare Committee (Regierungspräsidium Karlsruhe; Reference Nos. G-67/20, G-232/18, G-45/22, T22/21, and T49/21). All animal care and procedures concerning wild-type mice for RNA sequencing analysis conformed to the European Molecular Biology Laboratory guidelines for the Use of Animals in Experiments and were reviewed and approved by the Institutional Animal Care and Use Committee.

Control animals were compared with human sinus rhythm patients on action potential parameters and ion channel expression profiles. Inclusion criteria required that animals were in sinus rhythm and that tissue samples were of adequate size and quality for cell or RNA isolation. All available samples meeting these criteria during the defined project period were included in the study. In total, tissue samples from 9 mice, 4 rats, 12 pigs, and 8 horses were included in the study.

Cardiac tissue samples were obtained from C57BL/6N mice (aged 12–18 months) and Wistar rats (aged 15–20 months) of either sex. The mice and rats were housed in individually ventilated plastic cages under controlled environmental conditions (22±2 °C) with a 12-hour light/dark cycle. Rodents were provided with ad libitum access to food. After excision, hearts were rinsed in PBS (4 °C) and immediately dissected under a stereomicroscope (Stemi 2000; Zeiss, Germany). Cardiac compartments were identified according to anatomic landmarks. LA and RA tissue was transported in 2,3-butanedionmonoxime–containing cardioplegic solution, and either subjected to cardiomyocyte isolation within 30 minutes or directly flash-frozen in liquid nitrogen and stored at –80 °C.

German Landrace pigs (aged 4–6 months) were kept under specific pathogen-free conditions at a room temperature of 20±2 °C with a maximum housing density according to directive 2010/63/EU. Room lighting had a 12-hour light/dark cycle. Water was offered ad libitum and pigs were fed 2 times a day with balanced complete feed (SAF 130M; ZG Raiffeisen, Karlsruhe, Germany). Porcine hearts were explanted after euthanization in deep anesthesia: Following sedation with azaperone (5 mg/kg IM), midazolam (1 mg/kg IM), and ketamine (10 mg/kg IM), general anesthesia was induced with propofol (1.5 mg/kg IV) and sustained using isoflurane. Buprenorphine (0.02 mg/kg IV) was administered for analgesia. Euthanasia was performed by intravenous injection of 40 mL potassium chloride (1 mol/L). After excision, LA and RA tissue samples were either transported in 2,3-butanedionmonoxime–containing cardioplegic solution and subjected to cardiomyocyte isolation within 30 minutes or directly flash-frozen in liquid nitrogen and stored at –80 °C.

The horse tissue was obtained by our collaboration partners from Ghent University. Before euthanasia, horses were sedated with detomidine hydrochloride (10–20 μg/kg IV) followed by induction of general anesthesia with midazolam (0.06 mg/kg) and ketamine (2.2 mg/kg IV). Euthanasia was performed using a combination product (embutramide, mebenzonium iodide, tetracaine hydrochloride, 5 mL/50 kg IV). Immediately after euthanasia, atrial tissue samples were collected and sent to Heidelberg either flash-frozen at –80 °C for RNA isolation or in cardioplegic solution at 4 to 8 °C for cardiomyocyte isolation. Cell isolation and functional measurements of the equine cardiomyocytes were performed within 36 hours after organ removal.

Cardiomyocyte Isolation

As described above, heart tissue samples obtained from patients and various animals were kept in cardioplegic solution for transport and sample preparation. Connective and fatty tissue was cut off before small tissue samples were prepared for enzymatic digestion. The tissue was rinsed in EGTA-containing solution (in mmol/L: 137 NaCl, 5 KH_2PO_4, 1 $MgSO_4$, 5 HEPES, 10 glucose, 10 taurine, 0.2 EGTA; pH 7.4) for 5 minutes. Afterwards, samples were digested using collagenase type I (200 U/mL; Worthington Biochemical Corporation, Lakewood, NJ) and protease type XXIV (5.4 U/mL; Sigma-Aldrich, Steinheim, Germany). Digestion times were individually adapted for each species, ranging from 5 minutes for rodents to 30 minutes for horses. During the isolation procedure, all solutions were oxygenated with 100% O_2 at 37 °C. Supernatant was discarded, and the tissue was stirred in protease-free solution 3 times for 5 minutes, before suspensions were centrifuged for 2 minutes. Cell pellets were resuspended in a storage solution containing (in mmol/L) 10 EGTA, 25 glucose, 70 L-glutamic acid potassium salt monohydrate, 10 β-hydroxybutyrate, 20 KCl, 10 KH_2PO_4, 40 mannitol, 20 taurine, and 0.1% albumin (pH 7.4). Subsequently, cell suspensions were kept at room temperature while Ca^{2+} was reintroduced by gradually increasing the Ca^{2+} concentration to 2 mmol/L.

Cellular Electrophysiology

APs were recorded using the patch clamp technique in current clamp configuration. Patch pipettes were pulled from borosilicate glass (1B120F-4; World Precision Instruments, Berlin, Germany) and tip resistances consistently ranged from 3 to 8 MΩ. Pipettes were backfilled with internal solution containing (in mmol/L) 134 potassium D-gluconate, 6 NaCl, 1 MgATP, 1.2 $MgCl_2$, 10 HEPES (pH 7.2). Isolated cardiomyocytes were placed in external solution containing (in mmol/L) 137 NaCl, 5.4 KCl, 2 $CaCl_2$, 1 $MgSO_4$, 10 HEPES, 10 glucose (pH 7.3). Patch clamp recordings were conducted at room temperature. After obtaining a stable

GΩ seal, whole-cell ruptured patch configuration was reached by application of small manual suction pulses. Following compensation of the pipette capacitance, an average holding current density of −0.8 pA/pF was applied (Figure S1B). APs were elicited by injection of 10 brief current pulses (2 ms, threshold +50 pA) at 0.5 Hz stimulation rate.

RNA Sequencing

Human, equine, porcine, and murine atrial tissue samples were collected as described above and flash-frozen in liquid nitrogen. Samples were kept at −80 °C before tissue parts were homogenized using a TissueRuptor (QIAGEN, Hilden, Germany) system. The total RNA fraction was isolated using TRIzol Reagent (Invitrogen, Thermo Fisher Scientific, Waltham, MA) according to the manufacturer's instructions. Total RNA was subjected to poly(A)-enriched bulk RNA sequencing (Illumina NextSeq 2000 or Illumina HiSeq, 2×150 bp single index, 20–30 M reads/sample) by a commercial provider (Genewiz Germany GmbH, Leipzig, Germany). Bioinformatic analysis was performed using kallisto[13] for pseudoalignment and RStudio. Additionally, publicly available RNA sequencing data sets including atrial control tissue samples from rats (GSE201717,[14] GSE149542[15]) and humans (GSE112339,[16] GSE128188[17]) were downloaded and included in the analysis. Based on matrices containing transcripts per million (TPM) values, the data sets were integrated and filtered to retain only ion channel genes from predefined gene groups with documented cardiac expression and relevance to the AP. TPM values were then *Z*-score normalized within each sample to enable comparability of the relative ion channel expression profiles across data sets. Using these matrices for LA and RA samples, clustering analysis and heatmap visualization were performed. The clustering analysis was repeated both with and without the I_{KACh} gene group.

Computational Modeling

In 2 publicly available human RNA sequencing data sets,[16,17] genes encoding for channel subunits constituting the primary ionic currents incorporated in the single-cell computational model of Courtemanche et al[18] were identified. Genes contributing to the same ionic currents were grouped together as I_{Na}, I_{to}, I_{Kur}, I_{Kr}, I_{Ks}, and I_{K1}. TPM values were normalized, and the mean normalized TPM value for each current across both data sets was derived. By dividing the normalized TPM values by the mean value of the corresponding current, factors indicating the deviation from the mean value for each gene and sample were obtained.

The magnitude of an ionic current is directly proportional to its maximum channel conductance and, consequently, to the number of expressed ion channels. Assuming that gene expression levels associated with a specific ion channel are proportional to the number of expressed ion channels, and that the mean of each data set represents a healthy reference state for each current component, maximum channel conductance was scaled using the previously calculated factors of the gene expression data. Subsequently, single-cell simulations of the adapted models were performed using openCARP,[19] and AP parameters were extracted automatically.[20]

Data Acquisition

For the patch clamp experiments, Axopatch 200B, Axon Digidata 1550B, and pCLAMP 11 (Molecular Devices, San Jose, CA) were used for data acquisition and analysis.

Statistical Analysis

Statistical analysis was conducted using R Software version 4.2.0 (R Foundation for Statistical Computing, Vienna, Austria), RStudio 2022.02.2 (RStudio, Boston, MA) and Prism 10.4.0 (GraphPad, La Jolla, CA). Data are presented as mean±SEM. For comparisons between 2 groups, *P* values were derived from either unpaired Student's *t* tests or nested *t* tests. Welch's correction was applied when variances differed significantly between the groups. For experiments involving >2 groups, *P*-values were derived from generalized estimating equations with an exchangeable correlation structure, accounting for the nested data structure of cells within animals. Group differences were assessed using Dunnett's multiple comparisons procedure, with human as the reference group. $P<0.05$ was considered statistically significant. Specific details can be found in the figure legends.

RESULTS

Species-Specific Atrial AP Formation

The atrial AP can be divided into 5 phases (phase 0–4), characterized by distinct parameters. Phase 0 corresponds to the rapid depolarization of the transmembrane potential, primarily driven by the influx of sodium into the cell. Atrial depolarization can be quantitatively evaluated by the maximal upstroke velocity [$(dV/dt)_{max}$] and the AP amplitude (APA). Both the $(dV/dt)_{max}$ and the APA were highly comparable in human and porcine cardiomyocytes (58.2±2.2 V/s versus 59.1±3.0 V/s, $P=1.00$; 114.3±1.8 mV versus 120.3±2.7 mV, $P=0.31$), while both parameters were moderately increased in equine cells, and decreased in rodent cardiomyocytes (Figure 1A–1C).

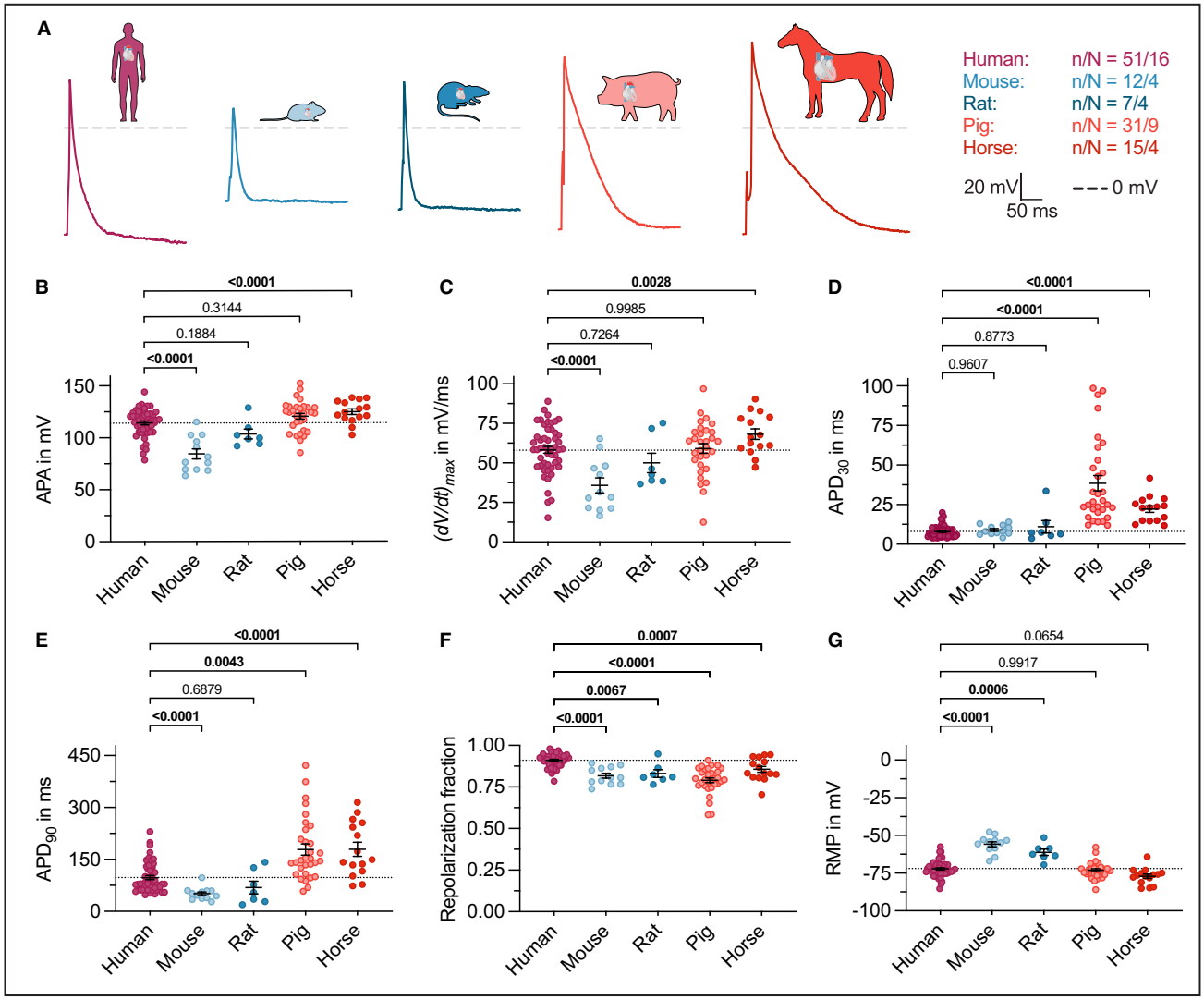

Figure 1. Atrial AP parameters in various species compared with human patients.
A, Representative AP traces recorded from atrial cardiomyocytes isolated from human, murine, rat, porcine, and equine tissue samples. The scale bar is depicted on the right. Number of cells (n) and number of animals (N) for the following AP parameters comparison are shown on the right (human: n/N=51/16; mouse: 12/4; rat: 7/4; pig: 31/9; horse: 15/4). **B**, APA in various species. **C**, Maximal upstroke velocity [$(dV/dt)_{max}$] in various species. **D**, APD_{30} in various species. **E**, APD_{90} in various species. **F**, Repolarization fraction [(APD_{90} – APD_{30})/APD_{90}] in various species. **G**, RMP in various species. Unless otherwise stated, data are shown as mean±SEM. Dotted lines mark the mean human value. Statistical comparisons were performed using generalized estimating equations with an exchangeable correlation structure, accounting for the nested data structure of cells within animals. Group differences were assessed using Dunnett's multiple comparisons procedure, with human as the reference group. $P<0.05$ was considered statistically significant. AP indicates action potential; APA, action potential amplitude; APD_{30}, action potential duration at 30% repolarization; APD_{90}, action potential duration at 90% repolarization; and RMP, resting membrane potential.

Phases 1 to 3 represent the repolarization of the membrane potential. Phase 1, the early repolarization, can be quantified by the AP duration (APD) at 30% repolarization (APD_{30}). The APD_{30} was particularly short in humans (8.0±0.5 ms) and prolonged in pigs (38.5±4.8 ms) (Figure 1D). Phase 2, the plateau phase, plays a significant role in ventricular cells, while it is less prominent in the atrial AP. Here, the plateau was more pronounced in porcine and equine APs compared with humans and rodents, which was represented by differences in the APD at 50% repolarization (APD_{50}) (Figure S1A). Phase 3, the final repolarization, can be quantified by the APD at 90% repolarization (APD_{90}). The APD_{90} was shortened in rodents (mice: 50.9±5.2 ms; rats: 69.0±18.4 ms) and prolonged in pigs and horses (178.6±16.2 ms; 179.4±20.3 ms) compared with human patients (97.5±5.9 ms) (Figure 1E). The repolarization fraction, defined as (APD_{90} – APD_{30})/APD_{90}, is a measure of the AP shape and the proportion of early and final repolarization. Here, the repolarization fraction was significantly higher in humans (0.91±0.006)

compared with all other species, indicating rapid early repolarization as a characteristic of the human atrial AP (Figure 1F).

Phase 4 corresponds to the resting membrane potential (RMP) of the cardiomyocyte, which was more depolarized in rodents, compared with human, porcine, and equine cardiomyocytes (Figure 1G).

In summary, rodents displayed a more depolarized RMP with decreased APA and $(dV/dt)_{max}$ compared with other species, while the human atrial AP was characterized by a rapid early repolarization and consecutively higher repolarization fraction. The APD_{90} increased with the animal size, with humans ranging between rats and pigs.

Of note, we chose a uniform stimulation frequency for patch clamp measurements across species to facilitate direct comparability. To assess potential rate-dependent effects, we considered species-specific heart rates and restitution studies (Figure S2A). In an in silico analysis of steady-state restitution behavior in human atrial cardiomyocytes, AP parameters changed exponentially at stimulation frequencies exceeding 2 Hz (Figure S2B and S2C). APs did not repolarize completely, leading to decreased $(dV/dt)_{max}$, peak potential, and APDs compared with the regular heart rate (Figure S2C). In contrast, we observed a plateau-like behavior at stimulation frequencies <1 Hz, corresponding to stimulation frequencies below the regular heart rate, with only minor effects on AP parameters (Figure S2C). Considering that, among the investigated species, horses exhibit the lowest resting heart rate with ≈30 bpm, we set stimulation frequencies to 0.5 Hz for all patch clamp measurements to avoid pacing-induced perturbances. The largest interspecies difference in heart rate exists between horses and mice, with mice displaying an ≈16-fold higher resting heart rate. To specifically estimate the effects of such subphysiological pacing rates on AP recordings, we performed simulations using an established model of human atrial cardiomyocytes at 0.0625 Hz, corresponding to a 16-fold reduction compared with physiological heart rate conditions. Here, we observed minor differences in AP parameters at 0.0625 Hz (gray) compared with the regular heart rate (blue) (Figure S2C).

APD Is Correlated to Cardiomyocyte Size

During patch clamp recordings, brightfield images of the cardiomyocytes were obtained for morphological characterization. We observed an increase in the cell surface area, perimeter, and cell length with increasing size of the animal species from mice to horses (Figure 2A and 2B). Human atrial cardiomyocytes were found to be intermediate in size, falling between those of rats and pigs (Figure 2A and 2B).

Subsequently, we explored the relationship between cell size and APD and identified a significant correlation between the cell surface area and the APD_{90} across species (Figure 2C; r=0.4414, P<0.0001). No significant difference in the size of LA and RA cardiomyocytes was observed (Figure 2D).

Species-Specific Ion Channel Expression Profiles

To further explore the electrophysiological characteristics on the transcriptomic level, we developed a new approach to compare atrial ion channel expression profiles across species. A comprehensive literature search served to identify ion channel subunits with documented cardiac expression and relevance (Figure 3A).[10,21–33] Ion channel subunit genes were categorized into specific sodium, calcium, and potassium currents attributed to the respective phases of the atrial AP (Figure 3A and 3B). Multiple RNA sequencing data sets from atrial control tissue samples of mice, rats, pigs, horses, and human patients in sinus rhythm were compiled into a TPM value matrix, which was then filtered for the predefined ion channel genes. To ensure comparability across data sets and species, Z-score normalization was applied to TPM values within each individual sample. This approach enables a comparison of the relative relevance of current gene groups within individual samples. Subsequent cluster analysis was performed separately for LA and RA samples (Figure 3B; Figure S3).

The obtained relative ion channel expression profiles revealed that the I_{KACh} gene group was strongly pronounced in all animal species compared with human samples, particularly in rodents (Figure S3A). As a result, the expression profiles of mice, rats, pigs, and horses clustered together, while the human data sets formed a separate main cluster (Figure S3A). However, since I_{KACh} exhibits only minimal basal activity and becomes functionally relevant primarily under vagal stimulation in vivo, we excluded the I_{KACh} gene group in a second step of our analysis (Figure 3B). This adjustment led to a distinct separation into 2 main clusters: rodents versus pigs, horses, and humans (Figure 3B).

Species-specific characteristics were particularly evident in gene groups contributing to the repolarization phase (Figure 3A and 3B): Regarding the early repolarization, I_{Kur} genes were most prominent in humans and had only minimal representation in rodents. L-type calcium channel genes, essential for the plateau phase of the AP, showed higher relative expression levels in humans and pigs compared with rodents. Conversely, T-type calcium channel genes were more prominent in mice and rats. I_{Ks} genes, contributing to the repolarization in phase 2 to 3, were specifically prominent in the relative expression profile of porcine atrial samples. Regarding the final repolarization and stabilization of

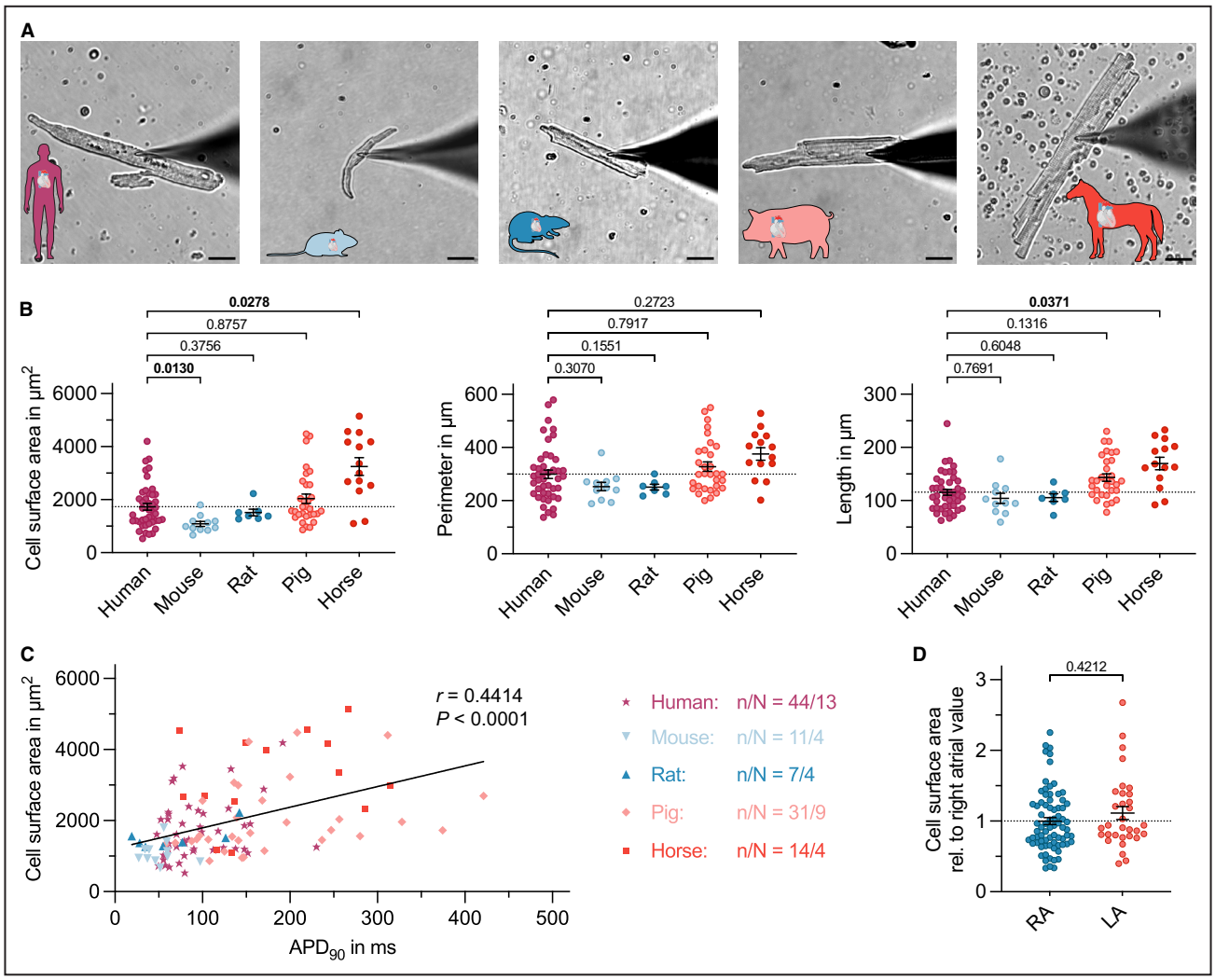

Figure 2. Cardiomyocyte morphology in various species compared with patients.
A, Representative images of cardiomyocytes isolated from human, murine, rat, porcine, and equine atrial tissue, acquired with brightfield microscopy during patch clamp experiments. The scale bars indicate 25 µm. **B**, Cell surface area, cell perimeter, and cardiomyocyte length of human, murine, rat, porcine, and equine atrial cardiomyocytes (human: n/N=44/13; mouse: 11/4; rat: 7/4; pig: 31/9; horse: 14/4). Dotted lines mark the mean human value. Statistical comparisons were performed using generalized estimating equations with an exchangeable correlation structure, accounting for the nested data structure of cells within animals. Group differences were assessed using Dunnett's multiple comparisons procedure, with human as the reference group. $P<0.05$ was considered statistically significant. **C**, Correlation of cell surface area and APD_{90}. A straight-line model was fitted with nonlinear regression, *r*- and *P*-values were derived from Pearson correlation. **D**, Cell surface area in RA and LA cardiomyocytes, shown relative to mean RA value of the respective species. *P* values were derived from a nested *t* test. $P<0.05$ was considered statistically significant. Unless otherwise stated, data are shown as mean±SEM. APD_{90} indicates action potential duration at 90% repolarization; LA, left atrial; and RA, right atrial.

the RMP, I_{K1} genes were prominent in horses and humans while markedly reduced in rodents.

The clustering pattern observed for LA samples was comparable to that described for the RA (Figure S3B and S3C). The I_{KATP} gene group played a more prominent role than in the RA samples, particularly in rat and porcine atria. Additionally, the characteristic prominence of I_{Kur} in the human expression profile was less pronounced in LA compared with RA samples (Figure 3B; Figure S3).

With that, we identified pronounced relevance of the I_{Kur} gene group as a characteristic feature of the human right atrial ion channel expression profile.

Correlation of Transcriptomic and Functional Electrophysiological Features

Next, we tested whether functional conclusions could be drawn from the relative ion channel expression profiles. In silico simulations of APs were conducted on the basis of the expression profiles and compared with

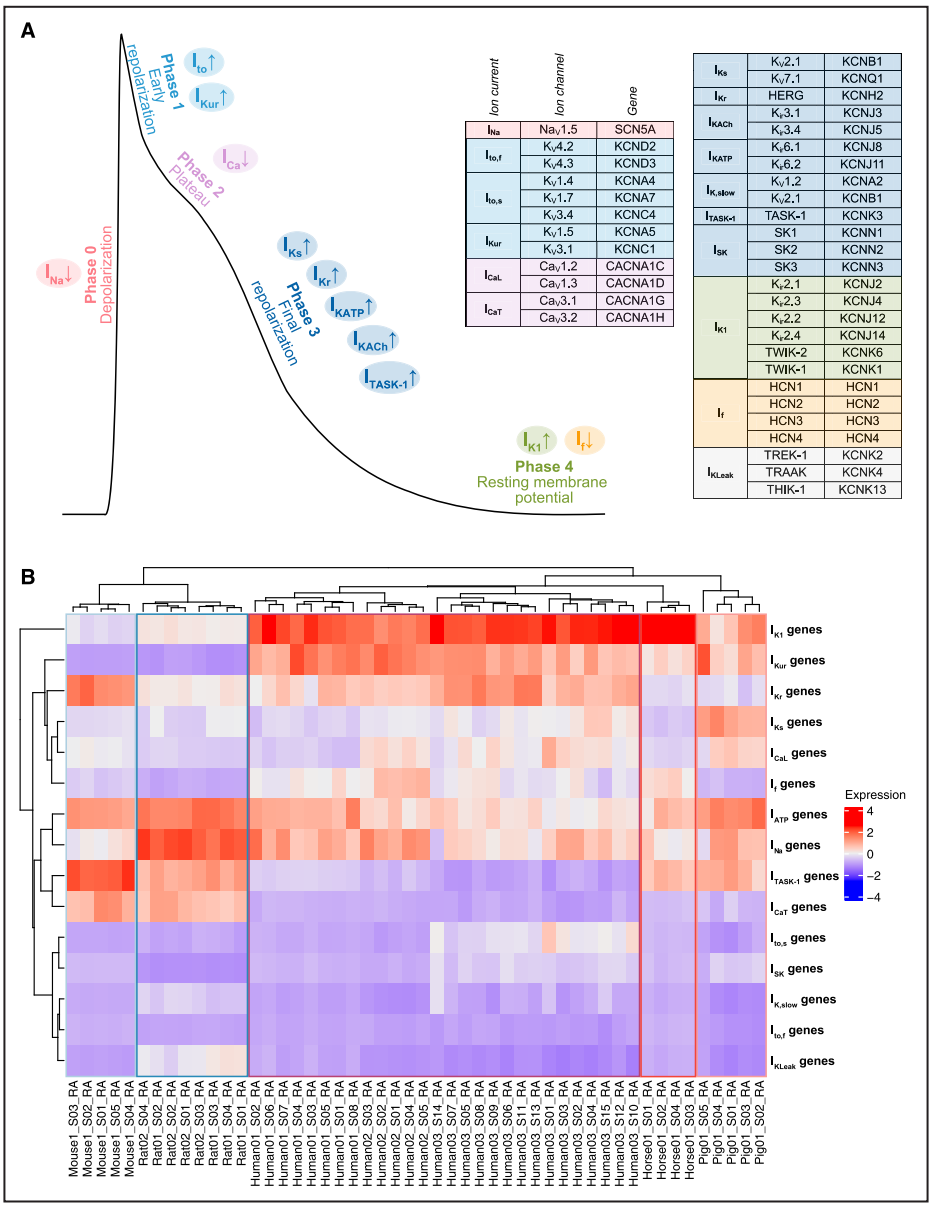

Ion current	Ion channel	Gene
I_{Na}	$Na_V1.5$	SCN5A
$I_{to,f}$	$K_V4.2$	KCND2
	$K_V4.3$	KCND3
$I_{to,s}$	$K_V1.4$	KCNA4
	$K_V1.7$	KCNA7
	$K_V3.4$	KCNC4
I_{Kur}	$K_V1.5$	KCNA5
	$K_V3.1$	KCNC1
I_{CaL}	$Ca_V1.2$	CACNA1C
	$Ca_V1.3$	CACNA1D
I_{CaT}	$Ca_V3.1$	CACNA1G
	$Ca_V3.2$	CACNA1H

I_{Ks}	$K_V2.1$	KCNB1
	$K_V7.1$	KCNQ1
I_{Kr}	HERG	KCNH2
I_{KACh}	$K_i3.1$	KCNJ3
	$K_i3.4$	KCNJ5
I_{KATP}	$K_i6.1$	KCNJ8
	$K_i6.2$	KCNJ11
$I_{K,slow}$	$K_V1.2$	KCNA2
	$K_V2.1$	KCNB1
I_{TASK-1}	TASK-1	KCNK3
I_{SK}	SK1	KCNN1
	SK2	KCNN2
	SK3	KCNN3
I_{K1}	$K_i2.1$	KCNJ2
	$K_i2.3$	KCNJ4
	$K_i2.2$	KCNJ12
	$K_i2.4$	KCNJ14
	TWIK-2	KCNK6
	TWIK-1	KCNK1
I_f	HCN1	HCN1
	HCN2	HCN2
	HCN3	HCN3
	HCN4	HCN4
I_{KLeak}	TREK-1	KCNK2
	TRAAK	KCNK4
	THIK-1	KCNK13

Figure 3. Species-specific ion channel expression profiles.
A, *Left*: Redrawn human atrial AP showing the phases of the AP and the contributing ion currents, respectively; *Right*: Ion channels and genes encoding for the respective subunits contributing to ion currents of the AP.[10,21–33] **B**, Heatmap and cluster analysis visualizing the relative ion channel expression profiles for human, murine, rat, porcine, and equine RNA sequencing data sets from RA tissue samples, after exclusion of the I_{KACh} gene group. AP indicates action potential; and RA, right atrial.

experimental data. As well-established in silico cardiomyocyte models are currently limited to human cells, we generated AP simulations on the basis of the human LA versus RA ion channel expression profiles and compared simulated and experimental AP parameters.

In patch clamp experiments, the APD_{30} and APD_{50} were significantly prolonged in LA compared with RA cardiomyocytes across species (APD_{30}: 1.30±0.10-fold prolongation, P=0.007; APD_{50}: 1.25±0.09-fold prolongation, P=0.023), while the APD_{90} remained unchanged (Figure 4A and 4B). This resulted in a reduced repolarization fraction in LA compared with RA APs (Figure 4A and 4B). All other quantified AP parameters showed no significant differences between LA and RA cells (Figure S4).

For the in silico approach, ionic conductance of the widely used Courtemanche model of human atrial cardiomyocytes[18] was scaled according to RNA sequencing data of human LA and RA tissue samples to estimate AP morphology. Consistent with

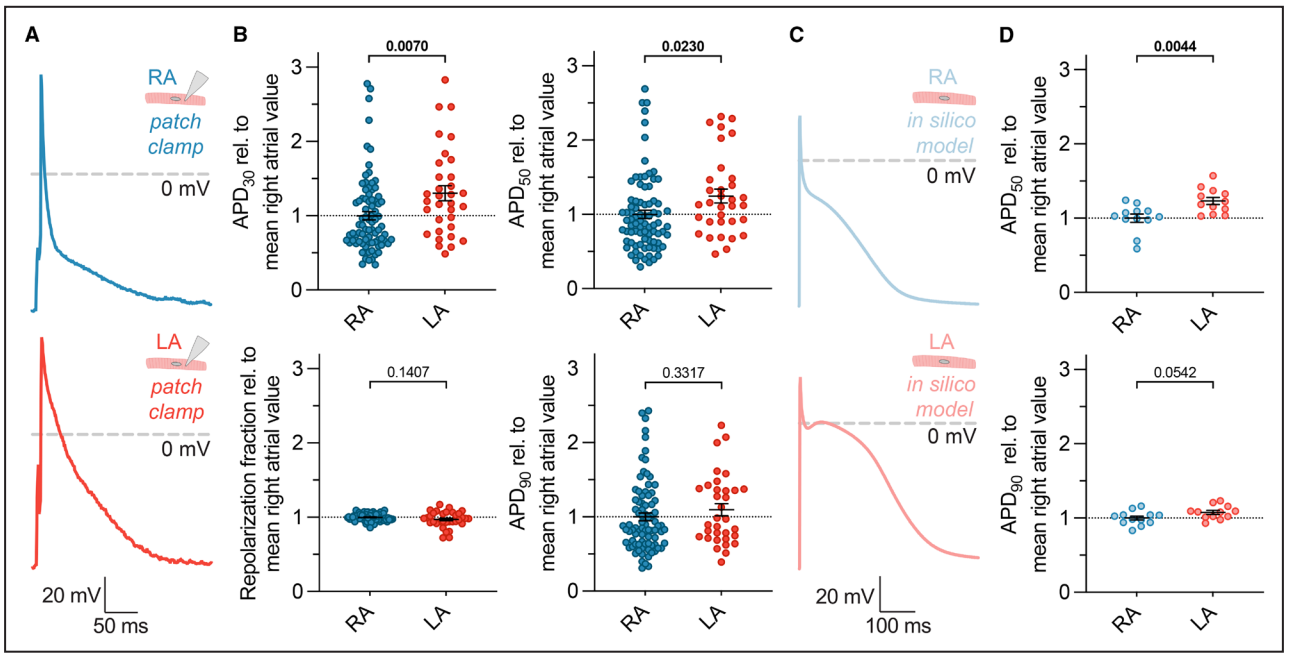

Figure 4. Differences between RA and LA APs across species.
A, Representative AP traces, recorded from human RA and LA cardiomyocytes. **B**, Subanalysis of AP recordings presented in Figure 1 and Figure S1: AP duration at 30%, 50%, and 90% repolarization (APD_{30}, APD_{50}, APD_{90}) and repolarization fraction in RA and LA cardiomyocytes. Human, murine, rat, porcine, and equine cardiomyocytes are pooled, and values are normalized to the RA mean of the respective species (human: n/N=51/16; mouse: 12/4; rat: 7/4; pig: 31/9; horse: 15/4). **C**, Representative AP traces, simulated on the basis of ion channel expression profiles obtained from RNA sequencing data of human RA and LA tissue samples. **D**, APD_{50} and APD_{90} of RA and LA APs relative to the RA mean value, simulated on the basis of 2 published RNA sequencing data sets (RA: n=13; LA: n=12). Unless otherwise stated, data are shown as mean±SEM. *P* values were derived from unpaired *t* tests. Welch's correction was applied when variances differed significantly between the groups. $P<0.05$ was considered statistically significant. AP indicates action potential; APD_{30}, action potential duration at 30% repolarization; APD_{50}, action potential duration at 50% repolarization; APD_{90}, action potential duration at 90% repolarization; LA, left atrial; and RA, right atrial.

experimental recordings, we observed no difference in APD_{90} (Figure 4C and 4D; Figure S5). The model appeared to inadequately capture APD_{30}, as a result of marked spike-and-dome morphology and generally short APD_{30}. However, APD_{50} and additionally assessed APD_{40} were consistently prolonged in the LA compared with the RA (Figure 4C and 4D; Figure S5). We found a 1.26±0.05-fold increase in the APD_{50} of LA compared with RA APs (Figure 4C and 4D), which was consistent with the experimental results. With that, the analysis served as a proof of principle that ion channel expression profiles can be linked to functional electrophysiological changes.

Sex-Specific Differences in AP Formation

Additionally, we compared sex-specific differences in AP formation across various species. In humans, the depolarization parameters APA and $(dV/dt)_{max}$ did not vary between female and male individuals (Figure 5A and 5B). However, we found significant differences in the repolarization phase, with the APD_{30} (12.1±1.3 ms versus 7.1±0.4 ms, $P=0.015$) and APD_{50} (24.3±3.2 ms versus 15.7±1.0 ms, $P=0.026$) being prolonged in female atrial cardiomyocytes (Figure 5A and 5C). Notably, the prolongation was more pronounced in early repolarization, as the APD_{90} (122.8±16.0 ms versus 92.1±6.1 ms, $P=0.066$) did not reach statistical significance. In pigs, these sex-specific differences in APDs were represented well (Figure 5D). In female individuals, the mean APD_{30} was prolonged by 75% (compared with 69% in humans) and APD_{50} by 55% (55% in humans) compared with male individuals (Figure 5C and 5D). In contrast, sex-specific differences in APDs were not represented in APs recorded from female and male murine cardiomyocytes (Figure 5E).

The clinical characteristics of female and male study patients are presented in Table S1. Regarding potential markers for atrial remodeling, there were no relevant differences in LA diameter and adjusted P-wave duration between female and male patients. Generally, we could not find any significant correlation between the single-cell APD_{90} or APD_{30} and the P-wave duration or the LA diameter within this cohort (Figure S6).

P-Wave Morphology in Pigs and Humans

In addition, atrial surface ECG parameters were compared between human patients and pigs in sinus rhythm (Figure 6A). Pigs exhibited a higher heart rate (human: 66.9±1.6 bpm; pig: 74.8±2.9 bpm; $P=0.020$), a shorter

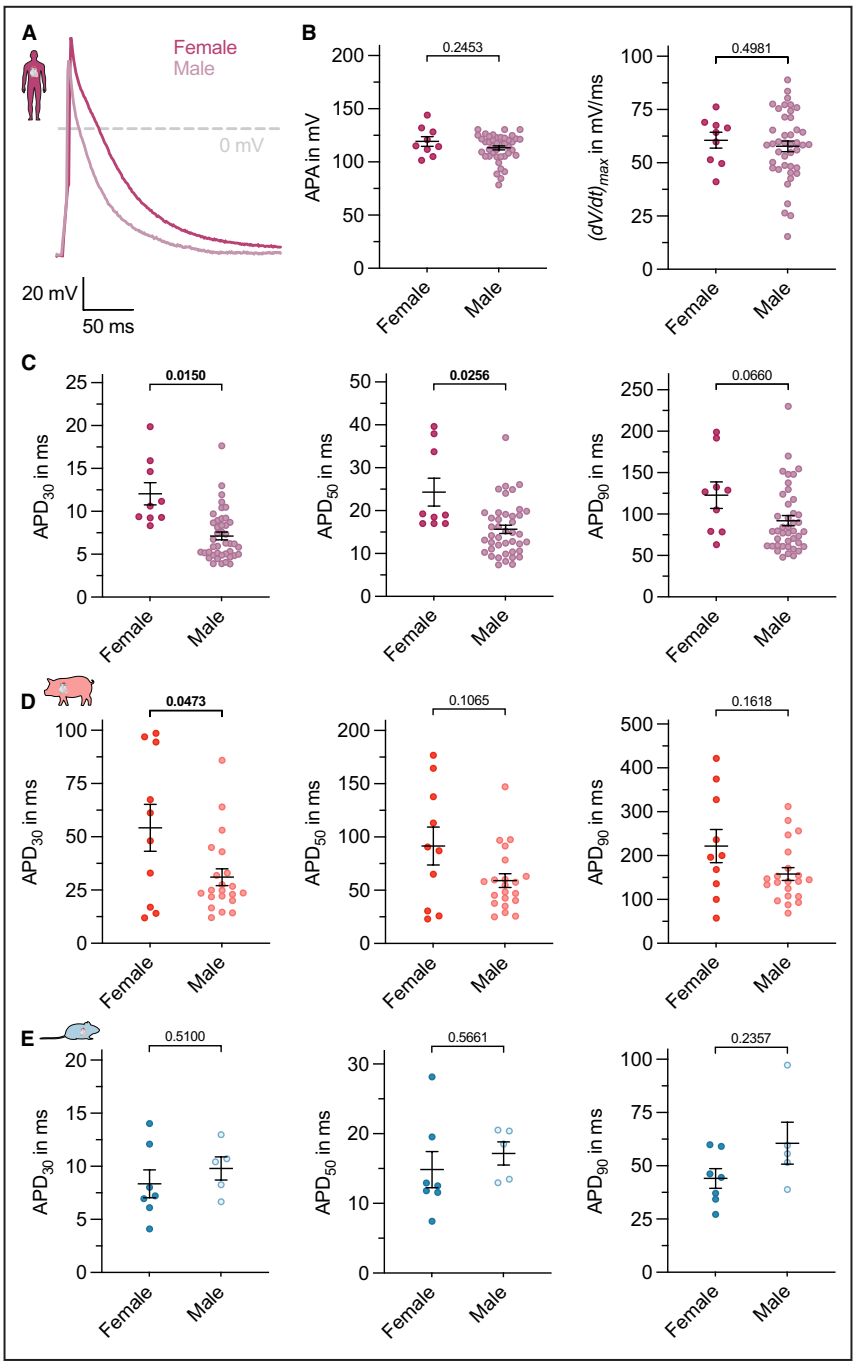

Figure 5. Atrial AP parameters in female and male individuals.
A, Representative AP traces recorded from atrial cardiomyocytes isolated from tissue samples obtained from female and male patients. The scale bar is depicted on the bottom. **B–E**, Subanalysis of AP recordings presented in Figure 1 and Figure S1: (**B**) AP amplitude (APA) and maximal upstroke velocity [$(dV/dt)_{max}$] in female (n=9 cells from N=4 individuals) and male (n/N=42/12) patients. **C**, AP duration at 30%, 50%, and 90% repolarization (APD_{30}, APD_{50} and APD_{90}) in female (n/N=9/4) and male (n/N=42/12) patients. **D**, APD_{30}, APD_{50} and APD_{90} in female (n/N=10/2) and male (n/N=21/7) pigs. **E**, APD_{30}, APD_{50} and APD_{90} in female (n/N=7/2) and male (n/N=5/2) mice. *P*-values were derived from nested *t* tests. $P<0.05$ was considered statistically significant. Unless otherwise stated, data are shown as mean±SEM. AP indicates action potential; APD_{30}, action potential duration at 30% repolarization; APD_{50}, action potential duration at 50% repolarization; APD_{90}, action potential duration at 90% repolarization; LA, left atrial; and RA, right atrial.

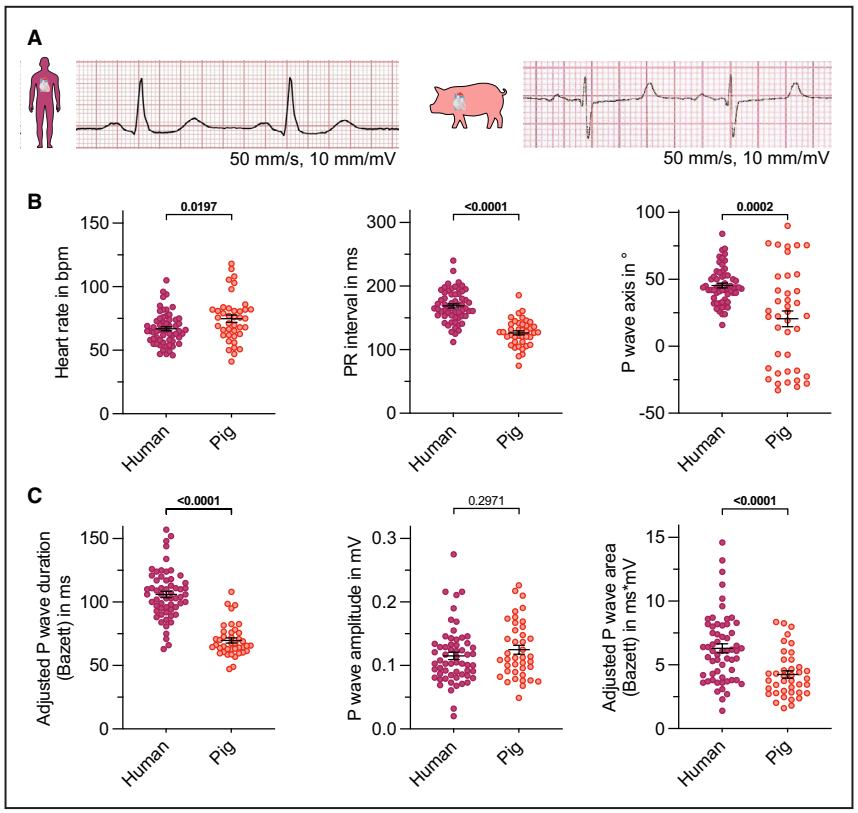

Figure 6. P-wave morphology in humans and pigs.
A, Representative surface ECG recordings (lead II) from humans (n=59) and pigs (n=35). **B**, Heart rate, PR interval, and P-wave axis in humans and pigs quantified from surface ECGs. **C**, Adjusted P-wave duration (Bazett), P-wave amplitude, and adjusted P-wave area (Bazett) in humans and pigs quantified from surface ECGs. Unless otherwise stated, data are shown as mean±SEM. *P* values were derived from unpaired Student's *t* tests. Welch's correction was applied when variances differed significantly between the groups. $P<0.05$ was considered statistically significant.

PR interval (human: 168.9±3.2 ms; pig: 126.4±3.3 ms; $P<0.0001$), and a significantly steeper P-wave axis (human: 45.4±1.8°; pig: 20.6°±5.9°; $P=0.0002$) (Figure 6B). With respect to the P-wave morphology, adjusted P-wave duration and area were relevantly reduced in pigs compared with humans, while P-wave amplitude did not vary significantly (Figure 6C).

DISCUSSION

Electrophysiological studies constitute an essential foundation in cardiac arrhythmia research. As the availability of human cardiac tissue is strongly limited, cellular electrophysiological investigations are commonly performed in animal models, despite well-recognized interspecies differences that may hinder the translation of experimental findings to clinical settings.[10,12] This limitation is particularly relevant in the context of pharmacological studies and the translation of new pharmacological approaches.[12,34,35] Recent reviews by Odening et al[6] and Schüttler et al[7] have improved the understanding of species-specific cardiac electrophysiology and established animal models of arrhythmia. However, comparisons across studies remain challenging due to methodological heterogeneity, and most available data focus on ventricular rather than atrial electrophysiology.

In this study, we combined cellular electrophysiology, transcriptomic profiling, and in silico modeling to characterize atrial electrophysiology across humans, mice, rats, pigs, and horses under standardized experimental conditions. Our results revealed that interspecies differences are phase specific. In particular, the representation of human electrophysiological properties in animal models differed between depolarization, early repolarization, and late repolarization phases. Furthermore, we highlighted additional layers of variability related to chamber- and sex-specific differences. Functional differences in AP characteristics could be linked to species-specific ion channel expression profiles, and a proof of principle in silico approach

supported a mechanistic connection between transcriptomic and electrophysiological properties.

Atrial depolarization differed between species, with a clear separation between rodents and large animals. Human depolarization characteristics were well reproduced in porcine atrial cardiomyocytes. In contrast, rodents exhibited reduced APA and $(dV/dt)_{max}$. Functionally, this can be attributed to a more depolarized RMP preceding the upstroke, which limits sodium channel availability. On the transcriptomic level, this observation corresponded to reduced relative expression of the I_{K1} gene group, which is relevant for the stabilization of the RMP.[10] Similar differences in RMP and I_{K1} density between rodents and humans have previously been described in ventricular cardiomyocytes.[23,36] In addition, rodents showed increased relative expression of T-type calcium channels, in line with reports that T-type calcium channel expression decreases with increasing body size of species, which may further contribute to a more depolarized RMP.[10,22,37] Absolute depolarization parameters must always be interpreted in the context of the experimental conditions. However, our findings highlight limitations of rodent models for studying depolarization-related mechanisms and support porcine cardiomyocytes as a more translationally relevant model for depolarization and class I antiarrhythmic effects.

Early repolarization characteristics emerged as a human-specific feature of atrial electrophysiology. Human atrial cardiomyocytes displayed a relatively short APD_{30} and a significantly higher repolarization fraction compared with all other species, indicating a rapid early repolarization resulting in a specific distribution between early and late repolarization phases. In line with the functional data, transcriptomic analysis suggested a greater relative importance of the I_{Kur} gene group in humans. The $K_V1.5$ potassium channel, encoded by *KCNA5* and primarily underlying I_{Kur}, is predominantly expressed in atrial tissue and has been widely investigated as an atrial-selective therapeutic target for AF.[38–44] However, experimental and clinical studies on I_{Kur} blockade have yielded inconsistent results,[10,41–43,45,46] and both $K_V1.5$ expression and functional effects of I_{Kur} inhibition vary across species and rhythm states.[21,42,43,45–49] Importantly, the characteristic early repolarization pattern observed in humans was not reproduced in the investigated animal models. In pigs, APD_{30} was substantially prolonged, which may additionally reflect a previously described reduced contribution of I_{to},[7,10,50,51] while rodents exhibited a more triangular AP with less distinct separation between early and late repolarization. The findings emphasize that human-specific early repolarization cannot be adequately reproduced in the investigated animal species and should preferentially be studied in human tissue.

Late repolarization, reflected by APD_{90}, generally scaled with animal size: Rodents exhibited shortened APs, whereas pigs and horses showed prolonged durations compared with humans. These interspecies differences largely reflect known variations in potassium currents underlying atrial repolarization.[6,7,11,12] In addition, our transcriptomic analysis indicated a reduced contribution of L-type calcium channels in rodents, further promoting AP shortening and triangularization.[6,36] Although APD_{90} differed across species, these differences were relatively small compared with much larger variations in physiological heart rates. This disparity translates into relevant differences in diastolic intervals and aligns with the observation that relative heart rate reserve is greater in large animals: Horses can increase their heart rate by ≈8-fold from rest, whereas mice exhibit only an ≈1.5-fold increase.

To enable direct comparability across species, all patch clamp recordings were performed at a uniform stimulation frequency of 0.5 Hz (BCL=2 seconds), corresponding to the resting heart rate of horses. In mice, this represents an ≈16-fold decrease relative to physiological rates, which could raise concerns about extrapolation to in vivo conditions. In silico simulations in a human atrial model, however, indicated that such subphysiological pacing rates have only minor effects on AP parameters. The observed steady-state restitution behavior of APD_{90} aligns well with experimental data from human atrial cardiomyocytes[52,53] and appears to be conserved across species.[54–56] Specifically, comparison of the subphysiological BCL of 2 seconds with species-specific resting BCLs—1 second in human atrial cardiomyocytes,[52,53] 0.86 seconds in porcine atrial cardiomyocytes,[54] 0.24 seconds in rat ventricular cardiomyocytes,[55] and 0.12 seconds in murine ventricular cardiomyocytes[56]—results in only minor differences in APD_{90}. Across species, steady-state restitution curves are shifted along the BCL axis, consistently placing the physiological resting BCL within the plateau region, such that longer BCLs yield similar APD_{90} values. These findings indicate that in healthy subjects under control conditions, AP behavior is predominantly governed by complete repolarization, and that, once attained, further increases do not lead to notable changes.

In vivo, heart rate and APD are modulated by multiple factors, including activation of I_{KACh}.[40,57–60] Vagal stimulation of I_{KACh} hyperpolarizes sinoatrial nodal cells, thereby reducing heart rate.[59,60] In atrial myocytes, I_{KACh} also contributes to phase 3 repolarization and may facilitate reentrant arrhythmias under conditions of elevated vagal tone. Moreover, constitutively active I_{KACh}-mediated AP shortening has been implicated in AF pathophysiology.[10,58,61] Given its predominantly atrial expression, I_{KACh}, similar to I_{Kur}, has been proposed as an atrial-selective therapeutic target. In our study, I_{KACh}

gene group expression was elevated in nonhuman species. In rodents, this may reflect a greater reliance on rapid, vagally mediated chronotropic adaption at higher heart rates. AF in mice is largely inducible only under vagal stimulation and cannot be induced in I_{KACh}-deficient mice,[61,62] supporting a potentially obligate role of I_{KACh} in rodent atrial vulnerability. In contrast, human atrial repolarization is shaped by a broader spectrum of repolarizing currents and pronounced relevance of I_{Kur}. Taken together, pharmacological I_{KACh} blockade may produce more pronounced antiarrhythmic effects in animal models than in clinical settings, which should be considered when translating findings from preclinical AF research.

Chamber-specific differences in atrial electrophysiology remain incompletely characterized and may vary across species and experimental conditions. Human data on RA versus LA comparisons are limited, as the majority of human patch clamp data have been obtained from RAA tissue. While shortened LA repolarization has frequently been reported in animal studies,[60,63–66] conflicting findings between single-cell and multicellular preparations have been reported.[66] In the present study, APD_{30} and APD_{50} were prolonged in LA compared with RA cardiomyocytes, whereas APD_{90} did not differ between chambers. Interestingly, it has been reported that I_{Kur} density is greater in RA compared with LA,[67] and reduced I_{Kur} has been linked to increased calcium transient amplitude and subsequent positive inotropic effects.[67,68] The observed prolongation in APD_{30} and APD_{50} may therefore correspond to higher mechanical demands of the LA operating against elevated left-cardiac pressures. Differential calcium handling may also carry implications for chamber-specific arrhythmogenesis. However, further dedicated studies are needed to systematically investigate region-specific atrial electrophysiology across species and experimental scales.

Sex-specific differences represent an additional layer of variability in atrial electrophysiology. In our human cohort, female patients exhibited prolonged APD compared with male patients, particularly during early repolarization. This finding was recapitulated in porcine cardiomyocytes but not in rodents, indicating species-dependent representation of sex differences. Previous studies, comprehensively reviewed by Prajapati et al,[69] have primarily focused on the ventricles, where repolarization is generally slower in women, as a result of reduced repolarizing currents and increased I_{CaL}.[69,70] Recent data from human atrial trabeculae demonstrated prolonged APD_{20} and APD_{50} but not APD_{90}.[71,72] The consistent prolongation of early repolarization in women suggests a robust sex-specific effect.[71–74] Given the higher prevalence of AF in men,[75] further investigation of sex-specific electrophysiological mechanisms is essential to determine pathophysiological and clinical implications. Here, our data raise awareness for differential representation of these sex-specific differences in animal models.

Finally, our study provides a proof of principle that functional electrophysiological properties may be inferred from transcriptomic data using in silico modeling. This approach is particularly attractive given the limited availability and complexity of patch clamp experiments and may enable the extraction of electrophysiological insights from existing RNA sequencing data sets. However, current in silico models are largely restricted to human cardiomyocytes, and reliable interspecies comparisons at this level require the development and validation of species-specific models. Encouragingly, recent advances in computational modeling suggest that this limitation will be addressed in the future.[12]

This study has further limitations. Human atrial tissue can only be obtained from individuals undergoing open heart surgery rather than from healthy subjects. Consequently, older patients were compared with younger and otherwise healthy animals. Although we aimed to include a relatively healthy subgroup without documented AF and only mildly altered left ventricular ejection fraction and LA diameter, all patients were of advanced age and had cardiac conditions requiring surgical intervention. Consequently, age- and disease-related remodeling of atrial tissue cannot be fully excluded and represents an inherent challenge in translational and preclinical electrophysiological studies. In addition, sample sizes were limited, particularly for the analysis of sex-specific differences. Technical factors must also be considered. Beyond the general limitations of in vitro recordings under artificial conditions, enzymatic cell isolation may alter cellular electrophysiological properties. To minimize potential effects on the interspecies comparison, experimental protocols were kept uniform across species. However, transport times for equine samples were substantially prolonged compared with other species, which may have further affected cellular properties. In this context, the selection of animal species was primarily determined by local availability. While the included species cover a broad range of physiological characteristics, other commonly used models in atrial arrhythmia research, such as goats, sheep, dogs, rabbits, and guinea pigs, were not assessed and may provide additional insights in future studies.

In conclusion, this study provides a comprehensive cross-species analysis of atrial electrophysiology, integrating functional and transcriptomic data. Our results demonstrate that human atrial electrophysiological properties are only partially recapitulated in commonly used animal models and differ between depolarization, early repolarization, and late repolarization. In addition, chamber- and sex-specific differences introduce further variability that is not consistently reflected across

species. By linking functional electrophysiological characteristics to ion channel expression profiles and demonstrating the potential of in silico modeling to derive functional insights from transcriptomic data, our study establishes a reference resource that enables the assessment of how well specific electrophysiological features and underlying ion channel mechanisms are represented across species. This enables more informed selection of animal models and a more accurate interpretation of experimental findings for translation to human atrial electrophysiology and arrhythmia research.

ARTICLE INFORMATION

Received December 29, 2025; accepted July 28, 2026.

Affiliations

Department of Cardiology, Heidelberg University Hospital, Im Neuenheimer Feld 410, D-69120, Heidelberg, Germany (A.P., F.W., C.G., L.W., M.K., M.J., N.F., C.S.); German Center for Cardiovascular Research (DZHK), Partner Site Heidelberg/Mannheim, University of Heidelberg, Im Neuenheimer Feld 669, D-69120, Heidelberg, Germany (A.P., F.W., C.G., L.W., M.K., M.J., N.F., C.S.); Department of Cardiology and Pneumology, University Medical Center Goettingen, Robert-Koch-Str. 40, D-37075, Goettingen, Germany (F.W., C.S.); DZHK, Partner Site Lower Saxony, University of Goettingen, Robert-Koch-Str. 42a, D-37075, Goettingen, Germany (F.W., C.S.); Institute of Biomedical Engineering (IBT), Karlsruhe Institute of Technology (KIT), Fritz-Haber-Weg 1, D-76131, Karlsruhe, Germany (C.G., A.L.); Equine Cardioteam Ghent, Department of Internal Medicine, Reproduction and Population Medicine, Faculty of Veterinary Medicine, Ghent University, Salisburylaan 133, B-9820, Merelbeke, Belgium (L.-M.V., A.D., G.v.L.); and Department of Cardiac Surgery, University Hospital Heidelberg, Im Neuenheimer Feld 410, D-69120, Heidelberg, Germany (A.L.M., M.Z., M.K.).

Acknowledgments

The authors thank Lisa Kuenstler, Katrin Kupser, Björn Rogatzki, Patricia Kraft, and Anne Grube for their excellent technical support.

Sources of Funding

German Cardiac Society Research Clinician–Scientist program (F.W.), German Heart Foundation/German Foundation of Heart Research (atrial fibrillation research funding to F.W. and C.S., F/03/19 to C.S., Kaltenbach scholarship to A.P.); German Centre for Cardiovascular Research (DZHK) (81X4500125, 81X4500132, 81X4500124, 81X4500117, and 81X4300142); German Ministry of Education and Research (BMBF); German Research Foundation (SCHM 3358/1-1 to C.S. and #507828355 to A.L.); Else-Kröner Fresenius Foundation (EKFS Fellowship and EKFS Clinician–Scientist professorship to C.S.); Zukunft-Niedersachsen research funding program; Helmholtz Association (HI-TAC tandem-project to C.S.). A.P., C.S., F.W., and M.K. are members of the CRC1425 and CRC1550, funded by the German Research Foundation (Nos. 422681845 and 464424253).

Disclosures

The authors declare that they have no competing interests.

Supplemental Material

ARRIVE Checklist
Table S1
Figures S1–S6

REFERENCES

1. Kornej J, Borschel CS, Benjamin EJ, Schnabel RB. Epidemiology of atrial fibrillation in the 21st century: novel methods and new insights. *Circ Res*. 2020;127:4–20. doi: 10.1161/CIRCRESAHA.120.316340
2. Van Gelder IC, Rienstra M, Bunting KV, Casado-Arroyo R, Caso V, Crijns HJGM, De Potter TJR, Dwight J, Guasti L, Hanke T, et al. 2024 ESC guidelines for the management of atrial fibrillation developed in collaboration with the European Association for Cardio-Thoracic Surgery (EACTS). *Eur Heart J*. 2024;45:3314–3414. doi: 10.1093/eurheartj/ehae176
3. Yang E, Vaishnav J, Song E, Lee J, Schulman S, Calkins H, Berger R, Russell SD, Sharma K. Atrial fibrillation is an independent risk factor for heart failure hospitalization in heart failure with preserved ejection fraction. *ESC Heart Fail*. 2022;9:2918–2927. doi: 10.1002/ehf2.13836
4. Kraft M, Buscher A, Wiedmann F, L'Hoste Y, Haefeli WE, Frey N, Katus HA, Schmidt C. Current drug treatment strategies for atrial fibrillation and TASK-1 inhibition as an emerging novel therapy option. *Front Pharmacol*. 2021;12:638445. doi: 10.3389/fphar.2021.638445
5. Andrade JG, Deyell MW, Macle L, Wells GA, Bennett M, Essebag V, Champagne J, Roux JF, Yung D, Skanes A, et al. Progression of atrial fibrillation after cryoablation or drug therapy. *N Engl J Med*. 2022;388:105–116. doi: 10.1056/NEJMoa2212540
6. Odening KE, Gomez AM, Dobrev D, Fabritz L, Heinzel FR, Mangoni ME, Molina CE, Sacconi L, Smith G, Stengl M, et al. ESC Working Group on cardiac cellular electrophysiology position paper: relevance, opportunities, and limitations of experimental models for cardiac electrophysiology research. *Europace*. 2021;23:1795–1814. doi: 10.1093/europace/euab142
7. Schüttler D, Bapat A, Kääb S, Lee K, Tomsits P, Clauss S, Hucker WJ. Animal models of atrial fibrillation. *Circ Res*. 2020;127:91–110. doi: 10.1161/CIRCRESAHA.120.316366
8. Schmidt C, Wiedmann F, Voigt N, Zhou XB, Heijman J, Lang S, Albert V, Kallenberger S, Ruhparwar A, Szabó G, et al. Upregulation of K(2P)3.1 K+ current causes action potential shortening in patients with chronic atrial fibrillation. *Circulation*. 2015;132:82–92. doi: 10.1161/CIRCULATIONAHA.114.012657
9. Iwasaki Y-k, Nishida K, Kato T, Nattel S. Atrial fibrillation pathophysiology. *Circulation*. 2011;124:2264–2274. doi: 10.1161/CIRCULATIONAHA.111.019893
10. Varró A, Tomek J, Nagy N, Virág L, Passini E, Rodriguez B, Baczkó I. Cardiac transmembrane ion channels and action potentials: cellular physiology and arrhythmogenic behavior. *Physiol Rev*. 2021;101:1083–1176. doi: 10.1152/physrev.00024.2019
11. Ripplinger CM, Glukhov AV, Kay MW, Boukens BJ, Chiamvimonvat N, Delisle BP, Fabritz L, Hund TJ, Knollmann BC, Li N, et al. Guidelines for assessment of cardiac electrophysiology and arrhythmias in small animals. *Am J Physiol Heart Circ Physiol*. 2022;323:H1137–H1166. doi: 10.1152/ajpheart.00439.2022
12. Morotti S, Liu C, Hegyi B, Ni H, Fogli Iseppe A, Wang L, Pritoni M, Ripplinger CM, Bers DM, Edwards AG, et al. Quantitative cross-species translators of cardiac myocyte electrophysiology: model training, experimental validation, and applications. *Sci Adv*. 2021;7:eabg0927. doi: 10.1126/sciadv.abg0927
13. Bray NL, Pimentel H, Melsted P, Pachter L. Near-optimal probabilistic RNA-seq quantification. *Nat Biotechnol*. 2016;34:525–527. doi: 10.1038/nbt.3519
14. Gams A, Brennan JA, Goldrick K, Efimov IR. Molecular and functional remodeling of superior and inferior SAN in a rat model of HCM. *JACC Clin Electrophysiol*. 2022;8:1341–1353. doi: 10.1016/j.jacep.2022.08.003
15. Brennan JA, Chen Q, Gams A, Dyavanapalli J, Mendelowitz D, Peng W, Efimov IR. Evidence of superior and inferior sinoatrial nodes in the mammalian heart. *JACC Clin Electrophysiol*. 2020;6:1827–1840. doi: 10.1016/j.jacep.2020.09.012
16. Johnson EK, Matkovich SJ, Nerbonne JM. Regional differences in mRNA and lncRNA expression profiles in non-failing human atria and ventricles. *Sci Rep*. 2018;8:13919. doi: 10.1038/s41598-018-32154-2
17. Thomas AM, Cabrera CP, Finlay M, Lall K, Nobles M, Schilling RJ, Wood K, Mein CA, Barnes MR, Munroe PB, et al. Differentially expressed genes for atrial fibrillation identified by RNA sequencing from paired human left and right atrial appendages. *Physiol Genomics*. 2019;51:323–332. doi: 10.1152/physiolgenomics.00012.2019
18. Courtemanche M, Ramirez RJ, Nattel S. Ionic mechanisms underlying human atrial action potential properties: insights from a mathematical model. *Am J Physiol*. 1998;275:H301–H321. doi: 10.1152/ajpheart.1998.275.1.H301
19. Plank G, Loewe A, Neic A, Augustin C, Huang YL, Gsell MAF, Karabelas E, Nothstein M, Prassl AJ, Sánchez J, et al. The openCARP simulation

environment for cardiac electrophysiology. *Comput Methods Programs Biomed*. 2021;208:106223. doi: 10.1016/j.cmpb.2021.106223
20. Goetz CPA, Wiedmann F, Kraft M, Prueser M, Frey N, Loewe A, Schmidt C. CAPPA: consistent analysis of action potential parameters for various types of cardiomyocytes. *Comput Cardiol*. 2024;51:4. doi: 10.22489/CinC.2024.273
21. Nerbonne JM, Kass RS. Molecular physiology of cardiac repolarization. *Physiol Rev*. 2005;85:1205–1253. doi: 10.1152/physrev.00002.2005
22. Melgari D, Frosio A, Calamaio S, Marzi GA, Pappone C, Rivolta I. T-type calcium channels: a mixed blessing. *Int J Mol Sci*. 2022;23:9894. doi: 10.3390/ijms23179894
23. Joukar S. A comparative review on heart ion channels, action potentials and electrocardiogram in rodents and human: extrapolation of experimental insights to clinic. *Lab Anim Res*. 2021;37:25. doi: 10.1186/s42826-021-00102-3
24. Schmidt C, Wiedmann F, Schweizer PA, Katus HA, Thomas D. Cardiac two-pore-domain potassium channels (K2P): physiology, pharmacology, and therapeutic potential. *Dtsch Med Wochenschr*. 2012;137:1654–1658. doi: 10.1055/s-0032-1305216
25. Zaveri S, Srivastava U, Qu YS, Chahine M, Boutjdir M. Pathophysiology of Ca(v)1.3 L-type calcium channels in the heart. *Front Physiol*. 2023;14:1144069. doi: 10.3389/fphys.2023.1144069
26. Schmitt N, Grunnet M, Olesen SP. Cardiac potassium channel subtypes: new roles in repolarization and arrhythmia. *Physiol Rev*. 2014;94:609–653. doi: 10.1152/physrev.00022.2013
27. Reilly L, Eckhardt LL. Cardiac potassium inward rectifier Kir2: review of structure, regulation, pharmacology, and arrhythmogenesis. *Heart Rhythm*. 2021;18:1423–1434. doi: 10.1016/j.hrthm.2021.04.008
28. Herrera-Perez S, Campos-Rios A, Rueda-Ruzafa L, Lamas JA. Contribution of K2P potassium channels to cardiac physiology and pathophysiology. *Int J Mol Sci*. 2021;22:6635. doi: 10.3390/ijms22126635
29. Scicchitano P, Carbonara S, Ricci G, Mandurino C, Locorotondo M, Bulzis G, Gesualdo M, Zito A, Carbonara R, Dentamaro I, et al. HCN channels and heart rate. *Molecules*. 2012;17:4225–4235. doi: 10.3390/molecules17044225
30. Biel M, Schneider A, Wahl C. Cardiac HCN channels: structure, function, and modulation. *Trends Cardiovasc Med*. 2002;12:206–212. doi: 10.1016/S1050-1738(02)00162-7
31. Torre E, Faure M, Bidaud I, Baudot M, Gaillardon M, Pereira de Vasconcelos W, Laarioui S, Talssi L, Engeland B, Reiken S, et al. L-type Ca(v)1.3 and HCN channels mediate heart rate acceleration by catecholamines. *Circ Res*. 2026;138:e327497. doi: 10.1161/CIRCRESAHA.125.327497
32. Singh H, Sanghvi SK. Top stories on intracellular potassium channels in cardiac arrhythmia. *Heart Rhythm*. 2024;21:2074–2075. doi: 10.1016/j.hrthm.2024.07.012
33. Yue L, Wang Z, Rindt H, Nattel S. Molecular evidence for a role of Shaw (Kv3) potassium channel subunits in potassium currents of dog atrium. *J Physiol*. 2000;527(Pt 3):467–478. doi: 10.1111/j.1469-7793.2000.00467.x
34. Van Norman GA. Limitations of animal studies for predicting toxicity in clinical trials: is it time to rethink our current approach? *JACC Basic Transl Sci*. 2019;4:845–854. doi: 10.1016/j.jacbts.2019.10.008
35. Van Norman GA. Limitations of animal studies for predicting toxicity in clinical trials: part 2: potential alternatives to the use of animals in preclinical trials. *JACC Basic Transl Sci*. 2020;5:387–397. doi: 10.1016/j.jacbts.2020.03.010
36. Blackwell DJ, Schmeckpeper J, Knollmann BC. Animal models to study cardiac arrhythmias. *Circ Res*. 2022;130:1926–1964. doi: 10.1161/CIRCRESAHA.122.320258
37. Ono K, Iijima T. Pathophysiological significance of T-type Ca^{2+} channels: properties and functional roles of T-type Ca^{2+} channels in cardiac pacemaking. *J Pharmacol Sci*. 2005;99:197–204. doi: 10.1254/jphs.FMJ05002X2
38. Li GR, Feng J, Yue L, Carrier M, Nattel S. Evidence for two components of delayed rectifier K+ current in human ventricular myocytes. *Circ Res*. 1996;78:689–696. doi: 10.1161/01.RES.78.4.689
39. Wang Z, Fermini B, Nattel S. Sustained depolarization-induced outward current in human atrial myocytes. Evidence for a novel delayed rectifier K+ current similar to Kv1.5 cloned channel currents. *Circ Res*. 1993;73:1061–1076. doi: 10.1161/01.RES.73.6.1061
40. Tamkun MM, Knoth KM, Walbridge JA, Kroemer H, Roden DM, Glover DM. Molecular cloning and characterization of two voltage-gated K+ channel cDNAs from human ventricle. *FASEB J*. 1991;5:331–337. doi: 10.1096/fasebj.5.3.2001794
41. Ellinwood N, Dobrev D, Morotti S, Grandi E. Revealing kinetics and state-dependent binding properties of I(Kur)-targeting drugs that maximize atrial fibrillation selectivity. *Chaos*. 2017;27:093918. doi: 10.1063/1.5000226
42. Wettwer E, Terlau H. Pharmacology of voltage-gated potassium channel Kv1.5—impact on cardiac excitability. *Curr Opin Pharmacol*. 2014;15:115–121. doi: 10.1016/j.coph.2014.02.001
43. Ford JW, Milnes JT. New drugs targeting the cardiac ultra-rapid delayed-rectifier current (I Kur): rationale, pharmacology and evidence for potential therapeutic value. *J Cardiovasc Pharmacol*. 2008;52:105–120. doi: 10.1097/FJC.0b013e3181719b0c
44. Blaauw Y, Gogelein H, Tieleman RG, van Hunnik A, Schotten U, Allessie MA. "Early" class III drugs for the treatment of atrial fibrillation: efficacy and atrial selectivity of AVE0118 in remodeled atria of the goat. *Circulation*. 2004;110:1717–1724. doi: 10.1161/01.CIR.0000143050.22291.2E
45. Pavri BB, Greenberg HE, Kraft WK, Lazarus N, Lynch JJ, Salata JJ, Bilodeau MT, Regan CP, Stump G, Fan L, et al. MK-0448, a specific Kv1.5 inhibitor: safety, pharmacokinetics, and pharmacodynamic electrophysiology in experimental animal models and humans. *Circ Arrhythm Electrophysiol*. 2012;5:1193–1201. doi: 10.1161/CIRCEP.111.969782
46. Kambayashi R, Hagiwara-Nagasawa M, Ichikawa T, Goto A, Chiba K, Nunoi Y, Izumi-Nakaseko H, Matsumoto A, Takahara A, Sugiyama A. Analysis of electropharmacological effects of AVE0118 on the atria of chronic atrioventricular block dogs: characterization of anti-atrial fibrillatory action by atrial repolarization-delaying agent. *Heart Vessels*. 2020;35:1316–1322. doi: 10.1007/s00380-020-01612-1
47. Ravens U, Wettwer E. Ultra-rapid delayed rectifier channels: molecular basis and therapeutic implications. *Cardiovasc Res*. 2011;89:776–785. doi: 10.1093/cvr/cvq398
48. Zicha S, Moss I, Allen B, Varro A, Papp J, Dumaine R, Antzelevich C, Nattel S. Molecular basis of species-specific expression of repolarizing K+ currents in the heart. *Am J Physiol Heart Circ Physiol*. 2003;285:H1641–H1649. doi: 10.1152/ajpheart.00346.2003
49. Dobrev D, Ravens U. Remodeling of cardiomyocyte ion channels in human atrial fibrillation. *Basic Res Cardiol*. 2003;98:137–148. doi: 10.1007/s00395-003-0409-8
50. Li GR, Du XL, Siow YL, O K, Tse HF, Lau CP. Calcium-activated transient outward chloride current and phase 1 repolarization of swine ventricular action potential. *Cardiovasc Res*. 2003;58:89–98. doi: 10.1016/s0008-6363(02)00859-3
51. Schultz JH, Volk T, Bassalay P, Hennings JC, Hubner CA, Ehmke H. Molecular and functional characterization of Kv4.2 and KChIP2 expressed in the porcine left ventricle. *Pflugers Arch*. 2007;454:195–207. doi: 10.1007/s00424-006-0203-1
52. Franz MR, Karasik PL, Li C, Moubarak J, Chavez M. Electrical remodeling of the human atrium: similar effects in patients with chronic atrial fibrillation and atrial flutter. *J Am Coll Cardiol*. 1997;30:1785–1792. doi: 10.1016/S0735-1097(97)00385-9
53. Van Wagoner DR, Pond AL, Lamorgese M, Rossie SS, McCarthy PM, Nerbonne JM. Atrial L-type Ca^{2+} currents and human atrial fibrillation. *Circ Res*. 1999;85:428–436. doi: 10.1161/01.res.85.5.428
54. Peris-Yague V, Rubio T, Fakuade FE, Voigt N, Luther S, Majumder R. A mathematical model for electrical activity in pig atrial tissue. *Front Physiol*. 2022;13:812535. doi: 10.3389/fphys.2022.812535
55. Hardy MEL, Pervolaraki E, Bernus O, White E. Dynamic action potential restitution contributes to mechanical restitution in right ventricular myocytes from pulmonary hypertensive rats. *Front Physiol*. 2018;9:205. doi: 10.3389/fphys.2018.00205
56. Knollmann BC, Schober T, Petersen AO, Sirenko SG, Franz MR. Action potential characterization in intact mouse heart: steady-state cycle length dependence and electrical restitution. *Am J Physiol Heart Circ Physiol*. 2007;292:H614–H621. doi: 10.1152/ajpheart.01085.2005
57. Wickman K, Krapivinsky G, Corey S, Kennedy M, Nemec J, Medina I, Clapham D. Structure, G protein activation, and functional relevance of the cardiac G protein-gated K+ channel, IKACh. *Ann N Y Acad Sci*. 1999;868:386–398. doi: 10.1111/j.1749-6632.1999.tb11300.x
58. Dobrev D, Friedrich A, Voigt N, Jost N, Wettwer E, Christ T, Knaut M, Ravens U. The G protein-gated potassium current I(K,ACh) is constitutively active in patients with chronic atrial fibrillation. *Circulation*. 2005;112:3697–3706. doi: 10.1161/CIRCULATIONAHA.105.575332
59. Park HJ, Georgescu SP, Du C, Madias C, Aronovitz MJ, Welzig CM, Wang B, Begley U, Zhang Y, Blaustein RO, et al. Parasympathetic

response in chick myocytes and mouse heart is controlled by SREBP. *J Clin Invest*. 2008;118:259–271. doi: 10.1172/JCI32011
60. Lomax AE, Rose RA, Giles WR. Electrophysiological evidence for a gradient of G protein-gated K+ current in adult mouse atria. *Br J Pharmacol*. 2003;140:576–584. doi: 10.1038/sj.bjp.0705474
61. Chang M, Gada KD, Chidipi B, Tsalatsanis A, Gibbons J, Remily-Wood E, Logothetis DE, Oberstaller J, Noujaim SF. I(KACh) is constitutively active via PKC epsilon in aging mediated atrial fibrillation. *iScience*. 2022;25:105442. doi: 10.1016/j.isci.2022.105442
62. Kovoor P, Wickman K, Maguire CT, Pu W, Gehrmann J, Berul CI, Clapham DE. Evaluation of the role of I(KACh) in atrial fibrillation using a mouse knockout model. *J Am Coll Cardiol*. 2001;37:2136–2143. doi: 10.1016/S0735-1097(01)01304-3
63. Wood MA, Mangano RA, Schieken RM, Baumgarten CM, Simpson PM, Ellenbogen KA. Modulation of atrial repolarization by site of pacing in the isolated rabbit heart. *Circulation*. 1996;94:1465–1470. doi: 10.1161/01.CIR.94.6.1465
64. Nygren A, Lomax AE, Giles WR. Heterogeneity of action potential durations in isolated mouse left and right atria recorded using voltage-sensitive dye mapping. *Am J Physiol Heart Circ Physiol*. 2004;287:H2634–H2643. doi: 10.1152/ajpheart.00380.2004
65. Qi A, Yeung-Lai-Wah JA, Xiao J, Kerr CR. Regional differences in rabbit atrial repolarization: importance of transient outward current. *Am J Physiol*. 1994;266:H643–H649. doi: 10.1152/ajpheart.1994.266.2.H643
66. Li D, Zhang L, Kneller J, Nattel S. Potential ionic mechanism for repolarization differences between canine right and left atrium. *Circ Res*. 2001;88:1168–1175. doi: 10.1161/hh1101.091266
67. Caballero R, de la Fuente MG, Gómez R, Barana A, Amorós I, Dolz-Gaitón P, Osuna L, Almendral J, Atienza F, Fernández-Avilés F, et al. In humans, chronic atrial fibrillation decreases the transient outward current and ultrarapid component of the delayed rectifier current differentially on each atria and increases the slow component of the delayed rectifier current in both. *J Am Coll Cardiol*. 2010;55:2346–2354. doi: 10.1016/j.jacc.2010.02.028
68. Grandi E, Pandit SV, Voigt N, Workman AJ, Dobrev D, Jalife J, Bers DM. Human atrial action potential and Ca^{2+} model: sinus rhythm and chronic atrial fibrillation. *Circ Res*. 2011;109:1055–1066. doi: 10.1161/CIRCRESAHA.111.253955
69. Prajapati C, Koivumaki J, Pekkanen-Mattila M, Aalto-Setala K. Sex differences in heart: from basics to clinics. *Eur J Med Res*. 2022;27:241. doi: 10.1186/s40001-022-00880-z
70. Gaborit N, Varro A, Le Bouter S, Szuts V, Escande D, Nattel S, Demolombe S. Gender-related differences in ion-channel and transporter subunit expression in non-diseased human hearts. *J Mol Cell Cardiol*. 2010;49:639–646. doi: 10.1016/j.yjmcc.2010.06.005
71. Pecha S, Ismaili D, Geelhoed B, Knaut M, Reichenspurner H, Eschenhagen T, Schnabel RB, Christ T, Ravens U. Resting membrane potential is less negative in trabeculae from right atrial appendages of women, but action potential duration does not shorten with age. *J Mol Cell Cardiol*. 2023;176:1–10. doi: 10.1016/j.yjmcc.2023.01.006
72. Ravens U. Sex differences in cardiac electrophysiology. *Can J Physiol Pharmacol*. 2018;96:985–990. doi: 10.1139/cjpp-2018-0179
73. Smith CER, Wang L, Guevara AM, Mott LR, Ni H, Grandi E, Ripplinger CM. Sex-specific electrophysiology and cholinergic responses underlie differential mechanisms of arrhythmia vulnerability in rabbit atria. *bioRxiv*. 2026;2026.02.18.706701. doi: 10.64898/2026.02.18.706701
74. Herrera NT, Ni H, Smith CER, Wu Y, Dobrev D, Morotti S, Grandi E. Mechanistic insights into sex differences in atrial electrophysiology and arrhythmia vulnerability through sex-specific computational models. *bioRxiv*. 2025;2025.08.18.670886. doi: 10.1101/2025.08.18.670886
75. Magnussen C, Niiranen TJ, Ojeda FM, Gianfagna F, Blankenberg S, Njølstad I, Vartiainen E, Sans S, Pasterkamp G, Hughes M, et al. Sex differences and similarities in atrial fibrillation epidemiology, risk factors, and mortality in community cohorts: results from the BiomarCaRE consortium (biomarker for cardiovascular risk assessment in Europe). *Circulation*. 2017;136:1588–1597. doi: 10.1161/CIRCULATIONAHA.117.028981